SPECTRAL SCALING OF THE 1985 TO 1988 NAHANNI, NORTHWEST TERRITORIES, EARTHQUAKES

By DAVID M. BOORE AND GAIL M. ATKINSON

ABSTRACT

The sequence of earthquakes that began in October 1985 near the Nahanni River, Northwest Territories, Canada, provides an exceptional opportunity to study the variation with magnitude of the source spectra from intraplate earthquakes. We study the spectral scaling for the seven largest events, using P waves recorded at stations of the Western Canada Telemetred Network (WCTN), the Eastern Canada Telemetred Network (ECTN), and the Global Digital Seismograph Network (GDSN). These earthquakes range in size from M = 4.8 to M = 6.8. We compare predictions from various source-scaling models with observed spectral ratios and source acceleration spectra for the suite of events. The spectral ratios show a strong azimuthal dependence, which is probably due to differences in the focal mechanisms or rupture characteristics of the events. Taking the average of the ratios from individual GDSN stations as the best representation of the spectral ratios, an ω-squared model with a constant stress parameter or one that increases slightly with moment magnitude gives a simultaneous fit to both the spectral ratios and to the absolute spectra. The high-frequency spectral levels, by themselves, imply a somewhat stronger dependence of the stress parameter on moment than found from fitting the overall spectra. The stress parameters for the scaling laws are less than 35 bars for earthquakes as large as M = 7. Recently proposed scaling laws in which the corner frequency is proportional to the inverse quarter root of seismic moment for an ω-squared model are not consistent with the data and neither are ω-cubed models.

The spectral scaling for the sequence of Nahanni earthquakes may not be representative of intraplate magnitude scaling in general, since there is some evidence that aftershocks do not exhibit the same scaling as main shocks. The high-frequency spectral levels of the aftershocks of both the Nahanni and the 9 January 1989 Miramichi, New Brunswick, earthquakes imply stress parameters that increase with magnitude. By contrast, the spectral levels for a series of main shocks in eastern North America show less magnitude dependence of the stress, and generally higher stress levels when compared to aftershocks of the same magnitude.

INTRODUCTION

A suite of moderate to large earthquakes occurred near the Nahanni River in the Northwest Territories of Canada during the last quarter of 1985 (with an additional event in 1988; see Table 1 for information about the events). Although they occurred in the western part of the continent, the Nahanni earthquakes have a number of characteristics similar to those of events in eastern North America: the events occurred in a region of compressive stresses, thrust mechanisms are dominant, surface ruptures are lacking despite shallow focal depths, and the rocks in the focal region have high seismic velocities. The motions from these events therefore may be relevant to engineering design in eastern North America (ENA) (Wetmiller *et al.*, 1988). Of particular interest to us is the study of the source scaling for these events, as a check on the scaling we assumed in deriving equations for the prediction of ground motion in eastern North America (Atkinson, 1984; Boore and Atkinson, 1987). The scaling we used—an ω-squared model with a stress parameter of 100

TABLE 1

NAHANNI EARTHQUAKES: LOCATIONS AND MAGNITUDES

Event	MM/DD/YY	HH:MM:SS	Latitude (N)	Longitude (W)	M_s	m_b	M
1	10/05/85	15:24:02	62.208	124.217	6.6	6.5	6.7
2	10/06/85	01:15:31	62.058	124.292		5.0	4.8
3	12/23/85	05:16:04	62.187	124.243	6.9	6.4	6.8
4	12/23/85	05:48:47	62.190	124.240		5.4	—
5	12/23/85	19:37:55	62.065	124.291	5.0	5.4	5.2
6	12/25/85	15:42:43	62.018	124.183	5.0	5.4	5.1
7	12/25/85	18:49:03	61.970	124.282	4.9	5.4	5.1
8	3/25/88	19:36:46	62.119	124.209	6.0	6.1	6.3

Epicenter information from Geological Survey of Canada (R. Wetmiller, personal comm., 1988, 1989).
M_s, m_b from ISC, except event 8, from NEIC.
M, moment magnitude, from our determinations of seismic moment.

bars—was consistent with the ENA data available at the time. None of the ENA earthquakes in our data set, however, was as large as the three largest Nahanni earthquakes (the largest of which was **M** = 6.8, where **M** is the moment magnitude); in fact, the ENA data came from events of marginal engineering significance.

It is fortunate that the Nahanni earthquakes were particularly well-recorded, at close distances on strong-motion accelerographs (Weichert et al., 1986), at regional distances by the Western Canada Telemetred Network (WCTN), and at teleseismic distances by the Eastern Canada Telemetred Network (ECTN) and the Global Digital Seismographic Network (GDSN). (For brevity, we include stations of the Regional Seismic Test Network (RSTN) within the GDSN designation.) Figure 1 shows the locations of the events and the recording stations. The average distance from the events to the WCTN stations is 1440 km (13°). The WCTN stations are contained within a circle of radius less than 200 km, and consequently the range of azimuths spanned by the network is small. The WCTN stations are close to PGC in Figure 1. The ECTN stations are 26° to 37° from the events; GAC in Figure 1 (at a distance of 32°) is part of the ECTN. We used records from 25 ECTN and 18 WCTN stations. The combined GDSN stations cover a wider azimuthal range than those from either the WCTN or ECTN, and therefore spectral ratios averaged over the GDSN stations are less likely to be biased by variations in radiation pattern or directivity from event to event.

Using techniques similar to those of Chael (1987), Chael and Kromer (1988), and Chun et al. (1989), we calculate spectral ratios of the events in the sequence, relative to the spectrum of the largest event. An advantage we have over the studies just mentioned is that the Nahanni events are large enough (**M** = 4.8 to **M** = 6.8) for us to estimate their seismic moments from teleseismic long-period recordings, thus removing some uncertainty in matching theoretical scaling relations with the observed ratios. Furthermore, estimates of the source acceleration spectrum for the largest Nahanni earthquakes have been made by Choy and Boatwright (1988), using data from the GDSN and the accelerograph recordings. We combine the spectral ratios with the acceleration spectrum estimated by Choy and Boatwright for the largest event to provide source acceleration spectra for the smaller events. This additional information reduces the ambiguity that results from interpretation of the spectral ratios alone.

DATA ANALYSIS

We use ratios between the spectra of particular events and a reference event (event 3) to estimate both the seismic moments and the source acceleration spectra
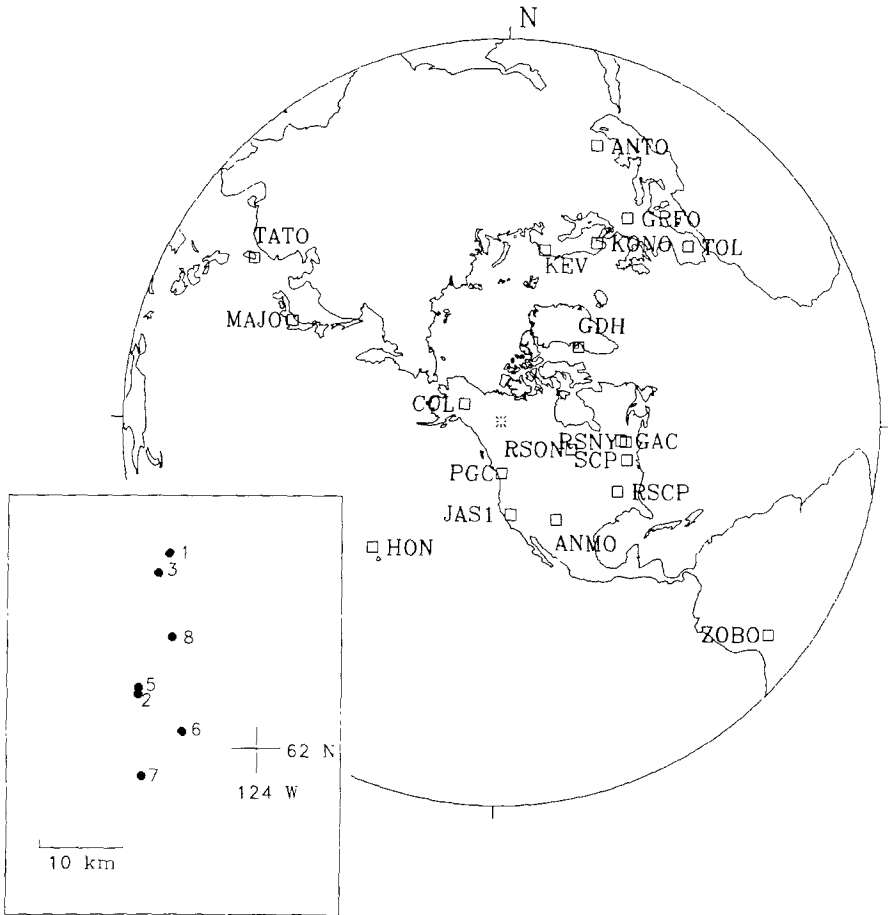
FIG. 1. Polar projection of the stations used to determine the spectral ratios and the seismic moments of the Nahanni earthquakes (the location of which is shown by the star at the center of the figure). To avoid clutter, individual WCTN and ECTN stations are not shown; the WCTN stations are near PGC, and GAC is an ECTN station. The inset shows the relative location of the events at a larger scale.

for the events. The basic assumptions in deriving these estimates and in fitting theory to the observations are that the earthquakes have the same location and that the focal mechanisms and the rupture characteristics (which control directivity effects) of the events are either all the same or that differences will not be important when averaged over all stations. The first assumption is only approximately true, with the epicenters of the larger events being 10 to 20 km north of the smaller events (Fig. 1). The depths of the events are poorly known for all but the largest events. The catalog of the International Seismological Centre, however, gives depths ranging from 6 to 10 km for all the events. This range of depths and the distances of 10 to 20 km between epicenters should not produce large variations in spectral excitation or differential attenuation, particularly at teleseismic distances, and we made no corrections to the observed spectral ratios to correct for these location differences.

Focal mechanisms from first-motion studies (Horner et al., 1990) show significant differences between events (Fig. 2). The first-motion mechanisms for the largest events (1, 3, and 8) are similar to those from waveform modeling of longer-period data (e.g., Choy and Boatwright, 1988, and moment-tensor solutions from Harvard and the U.S. Geological Survey, published in the *Preliminary Determination of*
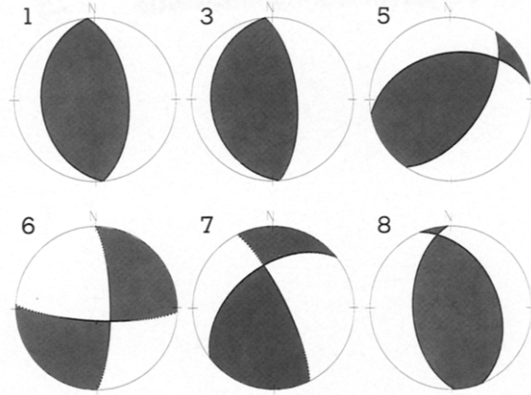
FIG. 2. Focal mechanisms from the Geological Survey of Canada (Horner *et al.*, 1990; R. Wetmiller, oral comm., 1989), plotted on the lower hemisphere of an equal-area stereonet. No mechanism is available for event 2. The dark areas have compressional first motions.

Epicenters of the National Earthquake Information Center). Event 5 is the only other event for which a moment-tensor solution has been published; that solution differs from the first-motion mechanism, but it is also more uncertain. In spite of uncertainties in the solutions, the assumption of similar radiation patterns is clearly not correct. We attempt to reduce the impact of these mechanism changes by averaging the estimates of spectral ratios and moments from stations widely distributed in azimuth.

Seismic Moments

Routine determinations of seismic moment (M_0) have been published for only four of the eight events that we have studied. The waveforms of event 4 at teleseismic distances are obliterated by the motions of event 3, and therefore a seismic moment could not be determined for event 4. For this reason we eliminated it from the study. In order to determine the moments of the remaining events, we scaled the moment of the largest earthquake in the sequence (event 3) by the relative amplitudes of similar phases for event 3 and the smaller events, recorded on long-period components of GDSN stations. This method allowed us to use a well-determined moment without having to do the computations, with their attendant assumptions, that are required by standard methods for moment estimation. We used Choy and Boatwright's (1988) moment for event 3; their moment is bracketed by the moments reported by others. The relative amplitudes were obtained from the long-period records, after we rotated them into transverse and radial components and filtered them with a low-pass filter having a corner period of 20 secs. The measurement of relative amplitudes was automated by using the crosscorrelation of the two traces, using a window containing the seismic wave of interest, divided by the autocorrelation of the reference event (with manual checks of the procedure). Window lengths depended on the station, and ranged from 120 to 190 sec for the S waves and 180 to 770 sec for the Love waves. For each wave type, we averaged the logarithm of the ratios over all stations for which the maximum of the correlation coefficient (Jenkins and Watts, 1968, p. 325) was greater than 0.7. The correlation of the waveforms is generally quite good, as illustrated in Figure 3. We averaged the log moment estimates obtained in this way for the SV and Love wave phases, with the results given in Table 2. The correlation of the SH waveforms is not as good as for

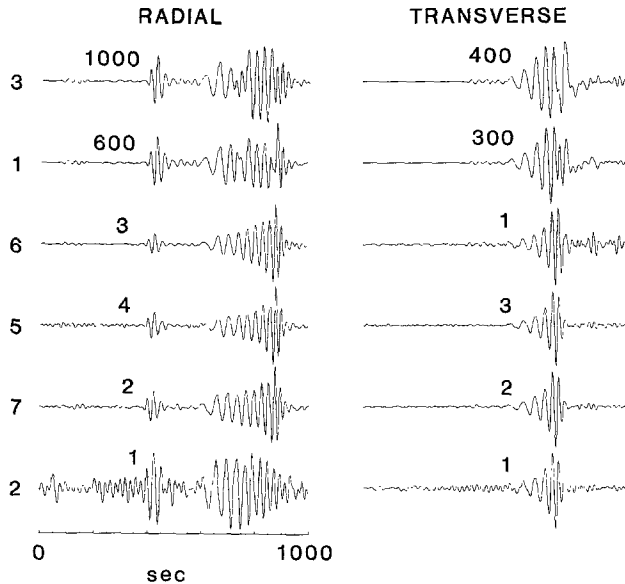RADIAL   TRANSVERSE

FIG. 3. Low-passed, rotated GDSN data used to determine seismic moments at station RSNY. The amplitude of each event relative to event 2 is given by the number above each trace. Note the high degree of correlation of the waveforms, particularly for the SV and Love waves; this was true at other stations and also for event 8, which was not recorded at RSNY. The relative moments were determined from the SV phase on the radial component and the Love waves on the transverse component.

TABLE 2

LOGARITHMS OF SEISMIC MOMENTS (IN DYNE-CM)

Event	Correlation	C & B	NEIC	Harvard	Estabrook	Wetmiller
1	26.06	26.08	26.04	25.92	26.12	26.00
2	23.32					
3	26.26	26.26	26.36	26.18	26.40	26.18
5	23.81			23.79		
6	23.77					
7	23.64					
8	25.49			25.40		

Correlation = estimated in this paper from relative amplitudes.
C & B = Choy and Boatwright (1988).
Estabrook = C. Estabrook (oral comm., 1988).
Wetmiller = Wetmiller et al. (1988).

the other phases, and therefore the SH phase was not used to estimate moments. The number of stations contributing to the average moment determined from the SV waves ranged from 4 for the smallest event (event 2) to 12 for event 8; for the estimates from the Love waves the number of stations ranged from 3 for event 2 to 8 for event 8.

The uncertainties in the moments derived for the smaller events are due to the uncertainty in the amplitude ratios and the uncertainty in the moment of the reference event, as well as effects of differing radiation patterns and rupture processes. The 95 per cent confidence limits on the logarithm of the ratios, as computed from the scatter about the mean values, are bounded by 0.1 log units, and the stated uncertainty in Choy and Boatwright's moment for event 3 is equivalent to 0.1 log units. We have combined these to estimate an uncertainty of 0.15 for the
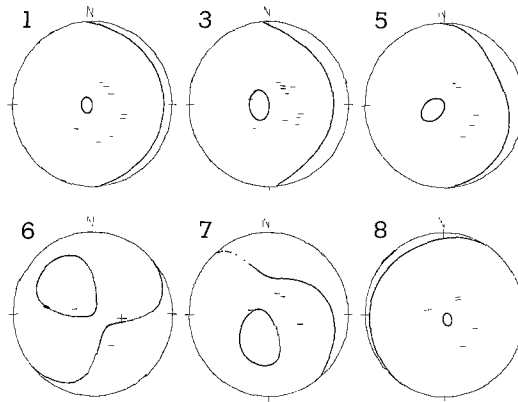
FIG. 4. Nodal planes of *SV* waves, using the Geological Survey of Canada focal mechanisms, plotted on the lower hemisphere of an equal-area stereonet. No mechanism is available for event 2. The symbols show those GDSN stations used in the determination of seismic moment, with the plus and minus indicating the predicted first-motion polarity (plus being motion away from the source).

logarithm of the seismic moments. Radiation pattern differences, mentioned earlier, are a matter of some concern, for it could lead to systematic biases in the moments. With the exception of event 6, the *SV* waves for the events are generally well away from the nodal surfaces for most stations (Fig. 4), and therefore their amplitudes should not be too sensitive to changes in focal mechanisms. Although not shown here, the same is not true for the *SH* waves, which may explain their poorer correlation. The stability of our results for various combinations of phases and components, as well as the comparison of our moments for events 1, 5, and 8 with those determined by more complete analyses (Table 2), indicates that our moment estimates are not strongly biased.

Spectral Ratios

The procedure we used for computing the spectral ratios closely follows that described by Chael (1987): power spectra were estimated by averaging the spectra obtained from overlapping, short segments of data, using the program SPCTRM in Press *et al.* (1986). A Parzen window was applied to each data segment to reduce spectral leakage. The total sample length for analysis ranged from 20 to 70 sec for the GDSN stations and was generally 60 sec for the WCTN and ECTN stations, beginning with the onset of the *P* wave. The ratios are for *P* waves; *S* waves are not available for as many stations and for frequencies as high as for *P* waves. In all cases, event 3 (the largest earthquake in the sequence) is used as the reference event. Data were deglitched as required. Spectra were computed using segment lengths from 2.1 to 8.5 sec, with shorter segments resulting in smoother spectral ratios. The smoothing results from averaging the spectra from overlapping time series; we did no additional smoothing of the spectra. Besides the smoothing, there were no systematic differences in the ratios for the various segment lengths, thus indicating that spectral leakage is minor. All results shown in this paper were computed using a length of 4.3 sec.

Power spectra are usually used when the signals are nearly stationary. While approximately true for WCTN stations, this is less so for the signals of the more distant GDSN and ECTN stations. We checked the results by obtaining Fourier

transforms for windows encompassing the dominant P-wave motions. The ratios formed from the smoothed Fourier amplitudes were very similar to those obtained from the square roots of the power spectral estimates. In this sense, the power spectra provide a convenient way to obtain smoothed estimates of the Fourier spectra (because the spectra are only used in ratios, the results are not sensitive to the duration of the windows).

We corrected the power spectra for noise by subtracting the noise power (computed using the portion of the record immediately before the signal) from the signal power. The logarithm of the square root of the ratio of the corrected power spectrum from each event relative to the reference event was averaged over all stations to form the final estimate. The spectral ordinate for a particular station, event, and frequency were included in the average only if the ratio of the corrected power spectrum of the signal to the noise power spectrum was greater than 4.0. The spectral ratios are not sensitive to the value of the lower limit; similar results were obtained with a lower limit of 0.0. Because of station-to-station variations in frequency dependence of the signal-to-noise ratios, only for the largest events did all stations provide data over the whole range of frequencies for which the average spectral ratios were determined. Records from WCTN and ECTN stations, sampled 60 times a second (except for GAC, with 30 samples/sec) generally produce usable spectral ratios at higher frequencies than do records from the GDSN, sampled 20 times a second (40 samples/sec for RSTN stations).

The computed spectral ratios, averaged over stations of the GDSN, ECTN, and WCTN, are shown in Figure 5. Note that the ordinate of our spectral ratio plots gives the square root of the ratio of power spectra rather than the ratio of power spectra, as shown by Chael (1987), Chael and Kromer (1988), and Chun et al. (1989). We prefer this, for it allows direct comparison with the ratio of the Fourier spectra of the radiated motion.

As with all the station-averaged spectral ratio data displayed in this paper, the portions shown are those for which the 95 per cent confidence limits of the mean logarithm of the ratios spanned less than 0.6 log units. The 95 per cent confidence limits include interstation variance but not the variance of the estimate at a single station.

In general, the spectral ratios in Figure 5 are in qualitative agreement with expectations from seismological models of source scaling. The ratios show an overall decrease in the ratio with decreasing frequency and have relative amplitudes that are consistent with the seismic moments, with the exception of event 1. Event 1 has a smaller seismic moment than event 3 (see Table 2), but it radiated more high-frequency energy (the difference is significant at the 95 per cent level). The difference in the relative excitation at low and high frequencies for events 1 and 3 is consistent with the long- and short-period magnitudes (M_s and m_b) reported by the International Seismological Centre (Table 1).

It is apparent from Figure 5 that the ratios from the WCTN data are systematically lower than those determined from the ECTN or the GDSN data. There seems to be a divergence toward long periods. The WCTN ratios may be affected by changes in the radiation patterns. The rays to the WCTN are nearly horizontal, at azimuths near 180°. As seen from Figure 2, such rays would have been near nodal planes for most of the events, and thus the spectral ratios may be sensitive to the differences in focal mechanisms between the larger and smaller events; the ratios at long periods may be more sensitive than at high frequencies, where scattering might blur the radiation pattern. We examine the possibility of an azimuthal bias
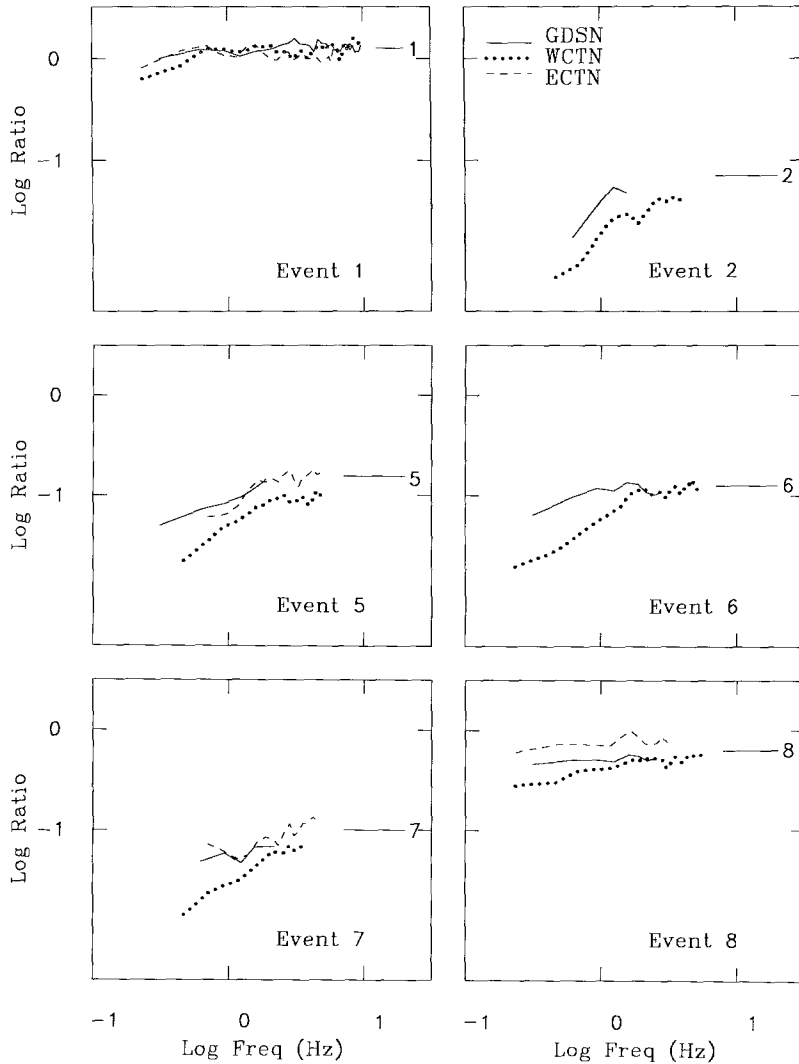
FIG. 5. Spectral ratios averaged over individual GDSN (lines), WCTN (dots), and ECTN (dashes) stations for the Nahanni events. The ratios were formed by dividing the square root of the power spectra, using event 3, as the reference event, in the denominator. Data for events 2 and 6 were not available from ECTN stations. Our estimates of the high-frequency levels of the spectral ratios are given by the short horizontal lines at the right of each graph.

affecting the spectral ratios in Figure 6, which shows the spectral ratios of event 6 at individual GDSN stations, arranged by azimuth. Observe that an azimuthal variation seems to be present, with the GDSN ratios for stations with southerly azimuths agreeing well with the WCTN ratios (at an azimuth close to 180°). This agreement suggests that ratios using data from WCTN stations have indeed been biased by radiation pattern effects. This is unfortunate since they are better resolved and cover a wider frequency band than do the ratios from the GDSN data.

We studied the spectral ratios at individual GDSN stations and found no anomalous stations that were strongly affecting the average ratios. (The spectral ratios for each event, at all GDSN stations used in our study, are given in Appendix A.) Furthermore, the ratios showed no obvious dependence on distance from the
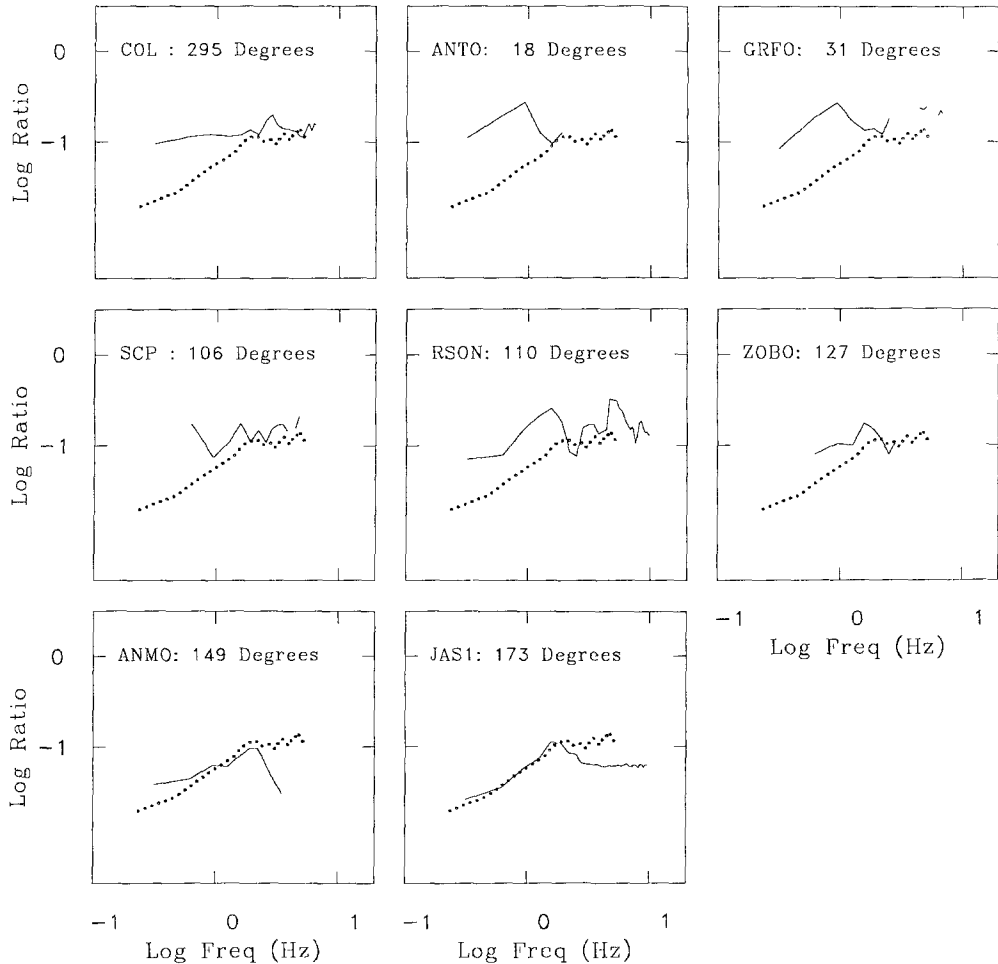
FIG. 6. Spectral ratios at individual GDSN stations, with the WCTN ratios for comparison (dots), for event 6. The ratios were formed by dividing the square root of the power spectra, using event 3, as the reference event, in the denominator. The stations have been arranged by source-station azimuth, clockwise from COL. Event 5 shows a similar pattern, even though it has a different focal mechanism (Fig. 2).

earthquakes to the stations. Such a distance dependence might be expected in view of the different mix of wave types comprising the P-wave signal at various distances. The signal will consist of a combination of direct- and surface-reflected P waves, S-to-P converted waves, various guided waves, or mantle reflections, depending on distance; at no distance beyond the immediate source region will the signal consist only of a direct P wave. Each of the wave types would probably sample a different part of the focal sphere, and this might lead to an effective averaging that would explain the insensitivity of the spectral ratios to recording distance. We conclude that the ratios from the GDSN data are representative of the average radiation from the source, and therefore subsequent interpretations will focus on the GDSN data. A summary of the station-averaged spectral ratios for all events used in our analysis is given in Figure 7a.

A useful quantity in the derivation of source-scaling relations is the high-frequency level of each spectral ratio. The ratios shown in Figure 5 seem to show some flattening at higher frequencies, and based on this figure and plots of the
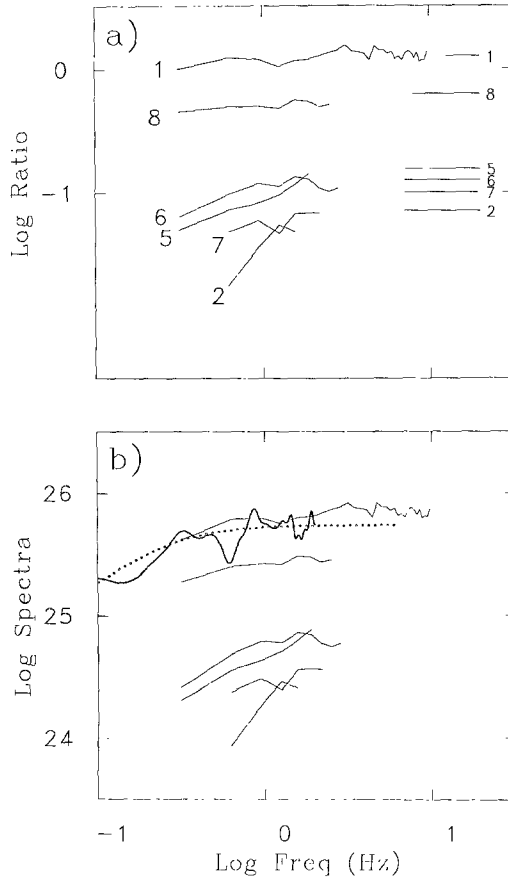
FIG. 7. Spectral ratios (*top*) and source acceleration spectra (*bottom*) from averages of ratios from GDSN stations. The ratios were formed by dividing the square root of the power spectra, using event 3, as the reference event, in the denominator. The source acceleration spectra were obtained by adding the logarithms of the ratios to the logarithm of a smoothed version (dotted line) of the acceleration spectrum determined by Choy and Boatwright (1988) for the reference event (heavy line). The Choy and Boatwright spectrum has been corrected for the $4\pi\rho\alpha^3$ source excitation factor, with $\rho = 2.7$ gm/cm^3 and $\alpha = 6.2$ km/sec, to make it directly comparable to $\omega^2 S(\omega)$, where $S(\omega)$ is the source displacement spectrum whose low-frequency level is the seismic moment (see equation (1) in the text); the units are dyne-cm/sec^2. Our estimates of high-frequency level for the ratios are shown on the right side of the top graph.

spectra at individual stations, we have estimated the spectral levels; the estimates are given by the short horizontal lines on the right sides of Figures 5 and 7a.

Source Acceleration Spectra

As we will show, the absolute levels of the acceleration spectra add important additional information that help reduce the uncertainties in source-scaling laws derived from the ratios alone. Source acceleration spectra for all events were estimated by adding the logarithms of the spectral ratios to a smoothed estimate of the logarithm of the spectrum for event 3; the event 3 spectrum was obtained by fitting a smoothly varying spectrum (equation B3) to the spectrum determined by Choy and Boatwright (1988). Figure 7b shows the Choy and Boatwright spectrum for event 3 (based on teleseismic data), the smoothed spectrum for that event, and the derived spectra for the other events. For most frequencies the construction of the acceleration spectra amounted to adding a constant to the log spectral ratios.

The absolute values of the spectra depend critically, of course, on the Choy and Boatwright (1988) estimates of the spectrum for event 3. Their acceleration spectrum is more susceptible to path and site variations than are the spectral ratios. A check on their teleseismically derived spectrum is the comparison of that spectrum with the spectrum calculated from the near-source accelerometer recordings. Figure 13 in Choy and Boatwright (1988) shows reasonable agreement between the two independent estimates of the source spectrum.

SOURCE-SCALING RELATIONS

The observed spectral ratios and source acceleration spectra provide an important means for evaluating various source-scaling relations. In this section, we compare the observed ratios and spectra to those computed from several published scaling relations. We also derive a scaling relation that fits the data better than do the published relations. Finally, we demonstrate the nonuniqueness associated with interpretation of the spectral ratios alone, particularly in the absence of information about the seismic moments of the earthquakes.

In our comparisons of theory and data, it is important to keep in mind the unusual scaling exhibited by the two largest events: the high-frequency energy shown by event 1 is greater than that of event 3, although the latter has a larger seismic moment. This switch in the relative amplitudes of low- and high-frequency spectral levels will not be predicted by any general source-scaling relations. When using derived scaling relations to predict ground motions, it should be recognized that the scaling relations attempt to describe in a simple way the behavior of a complex process. The scaling laws seem to work well when many events are considered, but because of variations in physical properties and in stress within the earth, any single event may have abnormal spectral content.

Theory

The equations describing the spectral ratios have been written in a convenient form by Chael and Kromer (1988); with a few exceptions we follow their notation here. The ratios are controlled by two factors: the shape of the source spectra, and the scaling law relating source corners to seismic moment. The source spectral amplitude for particle displacement from a point source can be described by

$$S(\omega) = \frac{M_0}{[1 + (\omega/\omega_0)^2]^{\gamma/2}} \tag{1}$$

where the constant γ controls the high-frequency decay of the spectra: $\gamma = 2$ and $\gamma = 3$ correspond to the ω-squared and ω-cubed models, respectively. The scaling law giving the relation of corner frequency ω_0 and seismic moment M_0 is expressed by

$$\omega_0 = kM_0^{-1/\delta}. \tag{2}$$

The parameter δ has been defined such that equation (2) can be rewritten as

$$M_0\omega_0^\delta = \text{constant}, \tag{3}$$

a form sometimes used in describing scaling relations. For example, constant-stress scaling is given by $\delta = 3$, and the Nuttli (1983) and Nuttli et al. (1987) scaling is

given by $\delta = 4$. The scaling for constant stress

$$M_0 \omega_0^3 \propto \Delta\sigma,$$

where $\Delta\sigma$ is the stress parameter, can be combined with the scaling law given by equation (2) to yield

$$\Delta\sigma \propto M_0^{(1-3/\delta)}. \tag{4}$$

When stress depends on moment ($\delta \neq 3$), the constant of proportionality in equation (4) can be determined by specifying a stress $\Delta\sigma'$ at a seismic moment M_0', according to

$$\left(\frac{\Delta\sigma}{\Delta\sigma'}\right) = \left(\frac{M_0}{M_0'}\right)^{1-3/\delta} \tag{5}$$

An alternate, more useful form of this equation in terms of moment magnitude $\mathbf{M}$, is

$$\log \frac{\Delta\sigma}{\Delta\sigma'} = \frac{3}{2}\left(1 - \frac{3}{\delta}\right)(\mathbf{M} - \mathbf{M}'). \tag{6}$$

In subsequent discussions, the reference moment has been chosen to be equivalent to a reference moment magnitude $\mathbf{M}' = 5.0$. With the above equations, the spectral ratio of an event with moment M_0 relative to a reference event of moment M_{0r} and corner frequency ω_{0r} can be written

$$R(\omega) = \left(\frac{M_0}{M_{0r}}\right)\left[\frac{1 + (\omega/\omega_{0r})^2}{1 + (M_0/M_{0r})^{2/\delta}(\omega/\omega_{0r})^2}\right]^{\gamma/2}. \tag{7}$$

The low-and high-frequency limits of the ratio are given by

$$R \rightarrow M_0/M_{0r} \tag{8a}$$

and

$$R \rightarrow (M_0/M_{0r})^{(1-\gamma/\delta)}, \tag{8b}$$

respectively. The latter equation is particularly useful, for it can be used to help constrain the appropriate scaling law by providing a direct estimate of the ratio γ/δ.

Comparisons to Published Scaling Laws

We used equation (7) to compute the spectral ratios corresponding to the moments of each of the Nahanni events. We make the assumption that the observed spectral ratios, made up of averages of various seismic waves, can be modeled by equation (7); we believe this is justified by the stability of the spectral ratios for individual GDSN stations (Appendix A). Different source-scaling relations were considered by

varying the frequency decay parameter and the amplitude scaling parameter δ. Figure 8 compares the observed spectral ratios to the predictions of several proposed source-scaling relations for intraplate earthquakes. These include those of Nuttli (1983), Nuttli et al. (1987), and relations deduced from the observations of Boatwright and Choy (1987; J. Boatwright, written comm., 1989). The Nuttli relations feature a stress parameter that increases with moment ($\delta = 4$, so that $\log \Delta\sigma \propto 0.38\mathbf{M}$) and an ω-squared spectral shape. The two Nuttli relations, which are given in Appendix B, differ in the stress parameter at the reference magnitude. The predictions of these relations can be calculated using equation (7). The Boatwright and Choy acceleration spectrum is proportional to ω^2 for frequencies below a corner frequency f_a and to ω^1 up to a second corner frequency f_b, above which the spectral amplitude is constant. The stress scaling of the Boatwright and Choy relations is approximately equivalent to constant stress. Because the Boatwright and Choy scaling has two corner frequencies, it cannot be modeled by equation (7). Our plotted predictions are based on the high-frequency spectral levels and corner frequencies (f_b) that Boatwright and Choy determined for a number of
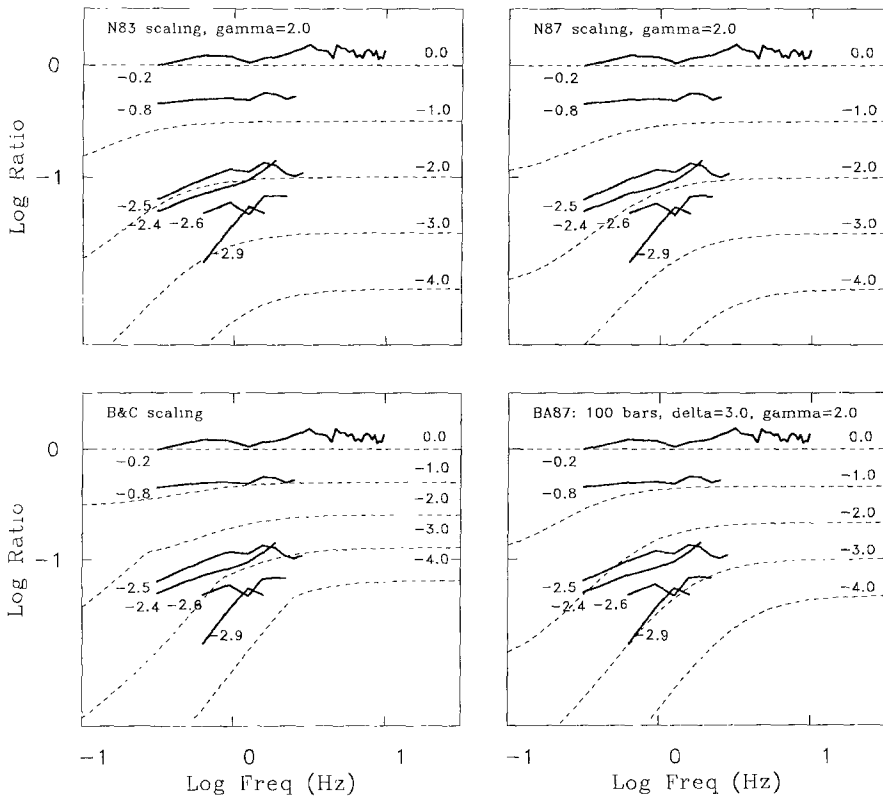

FIG. 8. Comparison of observed spectral ratios (solid lines) with theoretical ratios (dashed lines) for several source-scaling models proposed for intraplate earthquakes (N83: Nuttli, 1983; N87: Nuttli et al., 1987; B&C, Boatwright and Choy, 1987). Also shown are the ratios for the ω-squared, constant stress parameter model used by Boore and Atkinson (1987). "gamma" and "delta" refer to the scaling parameters defined in equations (1) and (2) in the text. The theoretical ratios have been computed for unit decrements in seismic moment from the moment of the reference event. This form of comparison is that used in previous studies of spectral ratios (Chael, 1987; Chael and Kromer, 1988; Chun et al., 1989) for which seismic moments of the events were not known. In our case these moments are known, and the difference between the logarithm of the moment for each event and the logarithm of the moment for the reference event is shown to the left of each observed ratio.

intraplate earthquakes. We derived a relationship for f_a that would satisfy both the intermediate-slope requirement and the required long-period level for the given seismic moment; the derived equations are given in Appendix B.

Examination of Figure 8 shows that with the exception of the smallest event, the shape of the spectral ratios matches the Nuttli (1983) and Nuttli et al. (1987) relations quite well; without information about the moments we might conclude that the ratios are consistent with the $\delta = 4$ scaling. (Previous studies of source scaling using spectral ratios, such as those of Chael (1987), Chael and Kromer (1988), and Chun et al. (1989), base their conclusions on plots such as these, without moment information.) The relative amplitudes of the events, however, are poorly matched by both Nuttli relations. The Boatwright and Choy relations are better, particularly at low frequencies. The last comparison in Figure 8 is with the model used in the Boore and Atkinson (1987) ground motion relations. This is an ω-squared model with a stress parameter of 100 bars. The shape does not fit the data as well as do the Nuttli relations, but the relative amplitudes are better predicted. ω-cubed models are not shown on the figure, but we show later that the ratios are also consistent with an ω-cubed model if stress increases sharply with moment. If the stress parameter is constant, the mismatch in shape for the ω-cubed model is similar to that found by Chael (1987), Chael and Kromer (1988), and Chun et al. (1989).

Fitting New Scaling Models to the Data

We show comparisons of the observed and calculated spectral ratios and acceleration spectra in Figures 9 and 10, respectively. Because of the limited bandwidth for which the spectral ratios were determined and the uncertainty associated with their shape, we chose not to invert the ratios and spectra directly for the parameters of the scaling relations. Instead, we used equation (8b) and the estimated high-frequency spectral levels to guide our choice of δ. We assume $\gamma = 2$ (ω-squared scaling) because of its past success in explaining many seismological observations (e.g., Hanks, 1979). For a given δ, we determined $\Delta\sigma'$ (the stress parameter for the reference moment, which corresponds to a moment magnitude of 5) by visually comparing theory and data for a suite of stress parameters. In choosing δ we used various averages of the high-frequency levels, emphasizing events 5 and 6 in one case and events 2 and 7 in another. The values of δ ranged between 3.0 (constant stress parameter) and 3.4; values of 3.0, 3.2, and 3.4 are shown in Figures 9 and 10. We also include $\delta = 4.0$; this value was found by Chun et al. (1989) in their analysis of spectral ratios for a suite of earthquakes near Miramichi, New Brunswick. This value of δ gives a much poorer fit to the data from the Nahanni earthquakes than do smaller values, however, and we will consider it no further.

Keeping in mind the possible uncertainty in the data, the fit to both the ratios and the acceleration spectra is generally adequate for $\delta = 3.0$, 3.2, and 3.4. The levels of the smallest events (in particular, event 2) are not predicted well, but overall we judge the predictions to be in reasonable agreement with the observations. In coming to this conclusion we considered the degree of fit between the theory and the observations, using a subjective weighting that gave more weight to events 5 and 6 than to the smaller events 2 and 7. We chose the values of $\Delta\sigma'$ independently in Figures 9 and 10 so as to give the best fit of the relative (Fig. 9) or absolute (Fig. 10) spectral levels; note that the values of $\Delta\sigma'$ are consistent only for the smaller δs. For example, $\Delta\sigma' = 20$ bars leads to a simultaneous fit of the theory to
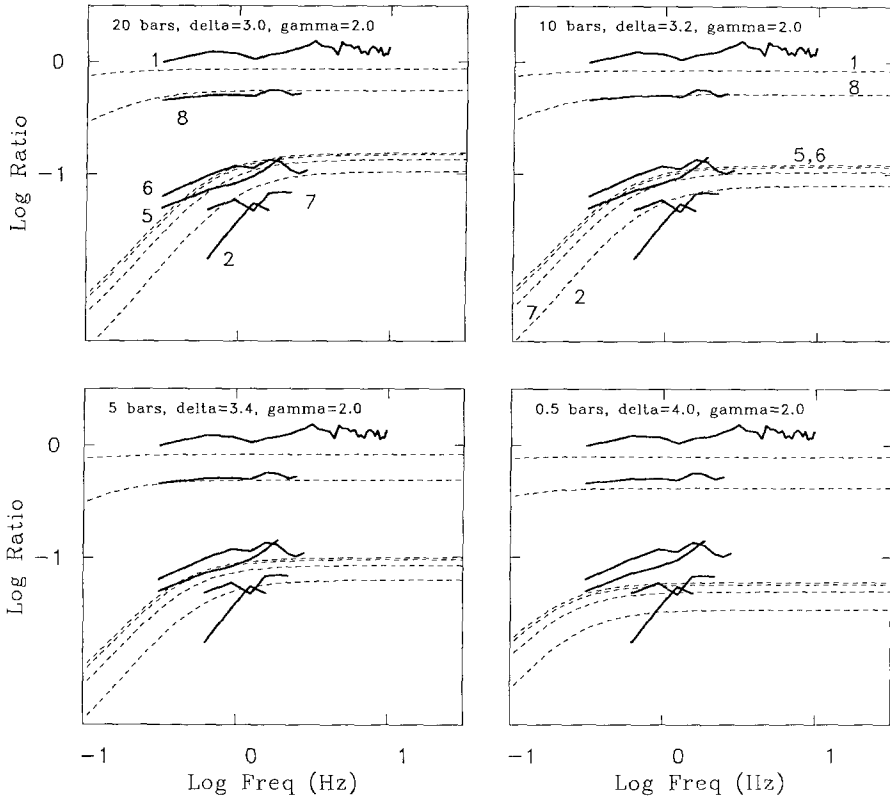
FIG. 9. Comparison of observed spectral ratios (solid lines) and theoretical ratios (dashed lines), for ω-squared models and scaling laws indicated by the delta and stress values shown in each graph (the stress values are those for a $\mathbf{M} = 5$ earthquake, and are equal to $\Delta\sigma'$ defined in equation (5)). The stress parameter was chosen by a subjective visual comparison of observed and theoretical ratios, using plots for a suite of stress parameters for each scaling law. These plots are not shown here. Unlike Figure 8, the actual moments for each event were used in the theoretical calculations.

both the observed spectral ratios and acceleration spectra when $\delta = 3.0$ (this is the case of a constant stress parameter), but for $\delta = 3.4$ the required stress parameter equals 5 and 15 bars for the spectral ratios and acceleration spectra, respectively. If forced to pick one model to represent the scaling of the Nahanni source spectra, we would choose $\delta = 3.1$ and $\Delta\sigma' = 15$ bars. From equation (6), this gives $\log \Delta\sigma \propto 0.05\mathbf{M}$. The fit of this model to both the spectral ratios and the acceleration spectra is shown in the left column of Figure 11.

We conclude this section with two more examples in which the acceleration spectra are helpful in eliminating models that are in good agreement with the spectral ratios. The first example is for an ω-cubed model, which can fit the spectral ratios if a strong dependence of moment is allowed. We show this in the upper graph of the middle column of Figure 11. Both the ω-squared model and the ω-cubed model can explain the spectral ratios equally well, and this is also true for many other combinations of the parameters and δ. As shown in the lower graph of the middle column, however, the ω-cubed model can be eliminated by use of the acceleration spectra. The extremely poor fit of the ω-cubed model to the absolute spectra is remarkable given how well the model fits the spectral ratio data. The second example concerns the scaling implied by the well-determined, but system-
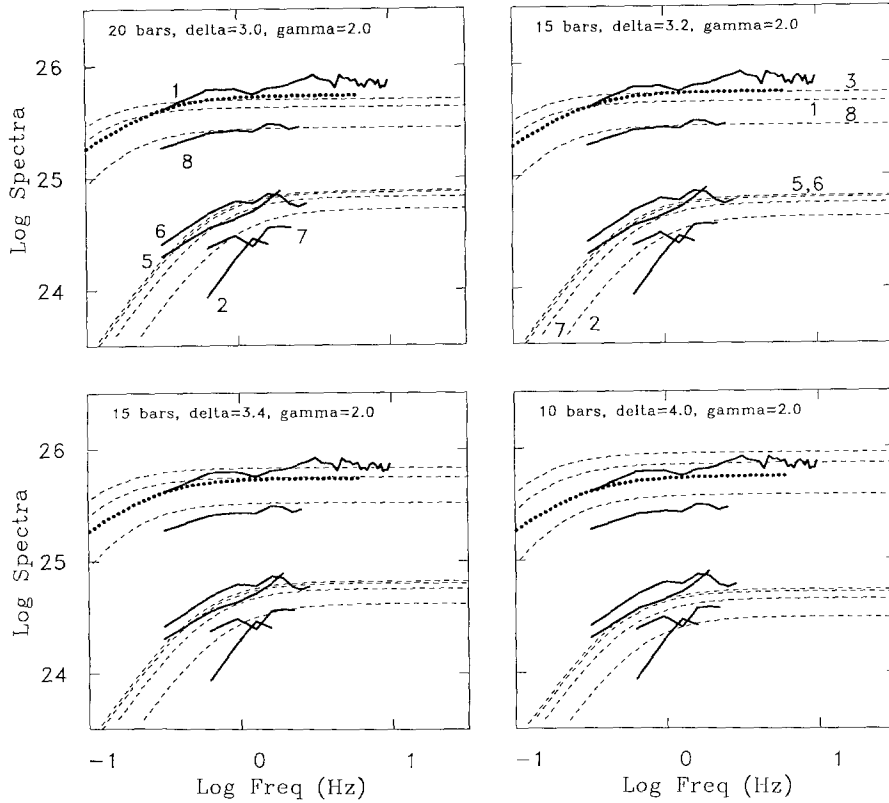
FIG. 10. Comparison of source acceleration spectra (solid lines, dotted for event 3) and theoretical spectra (dashed lines), for ω-squared models and scaling laws indicated by the delta and stress values shown in each graph (the stress values are those for a $\mathbf{M} = 5$ earthquake, and are equal to $\Delta\sigma'$ defined in equation (5)). The observations (solid lines) came from averages of the observations at individual GDSN stations. The dotted line is the smoothed version of the acceleration spectrum derived by Choy and Boatwright (1988) for event 3 (the reference event). The units of the acceleration spectra are dyne-cm/sec^2. The stress parameters were chosen by a subjective visual comparison of observed and theoretical spectra, using plots for a suite of stress parameters for each scaling law. These plots are not shown here. Unlike Figure 8, the actual moments for each event were used in the theoretical calculations.

atically biased, spectral ratios determined from the WCTN. As shown in the upper right graph of Figure 11, an ω-squared model with $\delta = 3.4$ and $\Delta\sigma' = 100$ bars fits the data very well (in fact, the fit seems better than the fit to the GDSN spectral ratios in the same figure). This scaling model, however, drastically overpredicts the absolute acceleration spectral levels, although the spectral shapes are approximately correct. The lesson from these examples is that caution is needed in drawing conclusions based strictly on spectral ratios.

SCALING OF HIGH-FREQUENCY ACCELERATION SPECTRA

The scaling laws used to fit the spectral ratios and acceleration spectra in Figures 9 and 10 imply various dependencies of the stress parameter on moment, ranging from no dependence for $\delta = 3.0$ to a strong dependence (log $\Delta\sigma \propto 0.38\mathbf{M}$) for $\delta = 4.0$. For all the models shown in Figures 9 and 10 the stress parameters are less than 60 bars for earthquakes smaller than $\mathbf{M} = 7$ (and they are less than 25 bars for the models with $\delta = 3.0$ and $\delta = 3.2$). This contrasts with the 100 bar stress parameter assumed in our published ground-motion predictions (Boore and
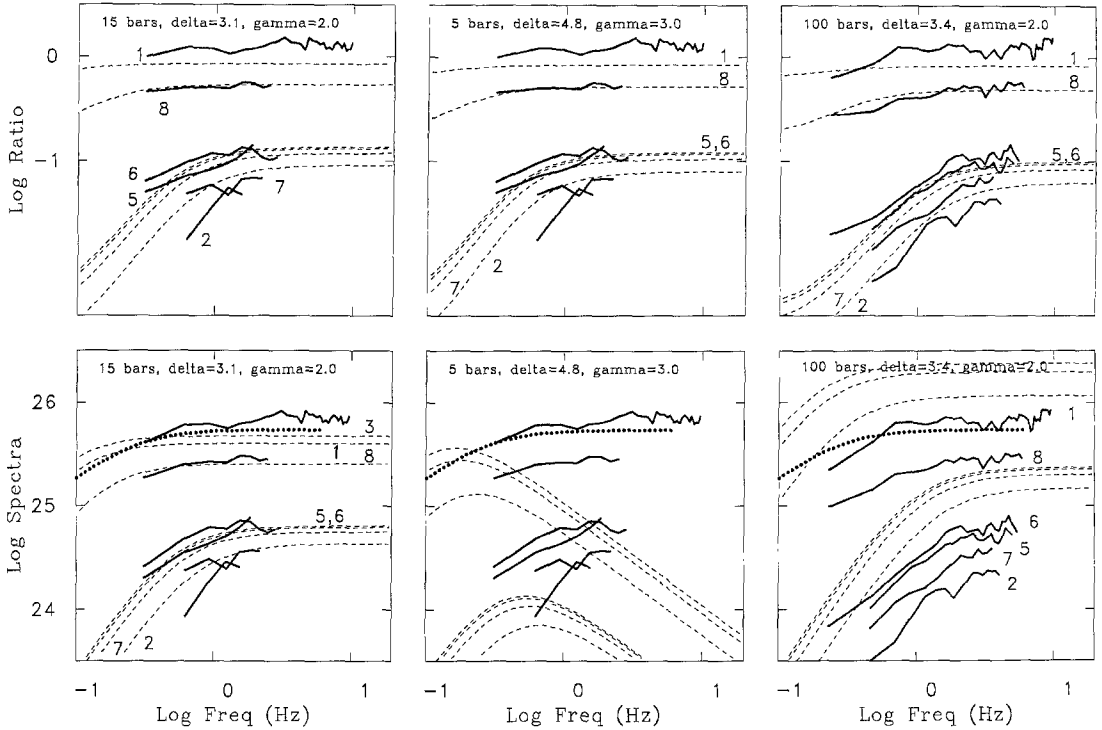
FIG. 11. Comparison of observed and theoretical spectral ratios (top graphs) and source acceleration spectra (bottom graphs). The observations (solid lines) came from averages of the observations at individual GDSN stations (left and middle columns) and WCTN stations (right column). The dotted line is the smoothed version of the acceleration spectrum derived by Choy and Boatwright (1988) for event 3 (the reference event). The units of the acceleration spectra are dyne-cm/sec^2. The scaling laws used in the theoretical calculations (dashed lines) are indicated by the stress, delta, and gamma values in each graph. ω-squared models were used in the left and right columns, and a ω-cubed model was used in the middle columns.

Atkinson, 1987). Differences in predicted ground motions for models with stress parameters of 25 and 100 bars are substantial for earthquakes large enough to be of engineering significance. To give some guidance as to the best stress parameter for use in predictions of ground motion in ENA, this section reviews ENA source acceleration spectra, at frequencies above the corner frequency. The ENA spectral levels are compared with those from the Nahanni earthquakes and with constant stress parameter scaling models. The advantage of using acceleration spectral levels is that teleseismic and regional data can be used to obtain estimates of source spectral levels for larger earthquakes, for which close-in data are lacking.

Figure 12 shows observed or derived high-frequency levels for ENA earthquakes, using the data listed in Table 3; also shown on the figure are the predicted levels for constant stress-parameter scaling. The data sources include regression analyses of recent moderate ENA earthquakes recorded by the Eastern Canada Telemetred Network (Atkinson, 1989), teleseismic analyses of large ENA events (Boatwright and Choy, 1987; J. Boatwright, written comm., 1988), analyses of large historical ENA events (Street and Turcotte, 1977), strong-motion data (Weichert et al., 1982), the results of this study, interpretation of the Miramichi aftershock studies of Chael (1987) and Chun et al. (1989), and preliminary results that we have obtained from ECTN and strong-motion recordings of the Saguenay earthquake (Boore and
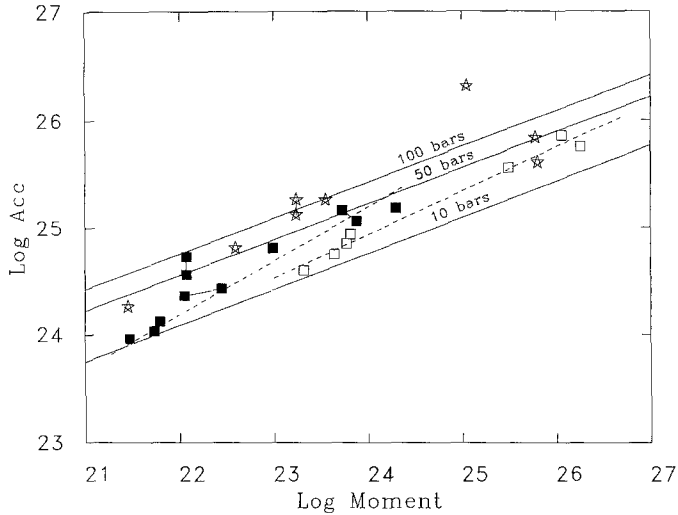
FIG. 12. High-frequency acceleration spectral levels for ENA and Nahanni earthquakes. Main shocks of all but the Nahanni and Miramichi earthquakes are given by stars; the Nahanni and Miramichi data are given by open and solid squares, respectively. See text for explanation of data and dashed lines. Units of acceleration spectra are dyne-cm/sec^2 (see caption to Fig. 7).

TABLE 3

SOURCE ACCELERATION SPECTRAL LEVELS

Date (MM/DD/YY)	Location	log M_0	log A	Reference
3/01/25	Charlevoix	25.80	25.60	Street & Turcotte (1977)
11/18/29	Grand Banks	25.78	25.83	Street & Turcotte (1977)
1/19/82	New Hampshire	22.59	24.81	Atkinson (1989)
10/07/83	New York	23.55	25.26	Atkinson (1989)
10/11/83	Ottawa	21.45	24.26	Atkinson (1989)
1/31/86	Erie	23.24	25.26	Atkinson (1989)
1/31/86	Erie	23.24	25.12	accelerograph record
1/09/82	Miramichi	24.30	25.18	Boatwright & Choy (1987)
1/09/82	Miramichi	22.99	24.81	spectral ratio
1/11/82	Miramichi	23.73	25.16	spectral ratio
1/11/82	Miramichi	23.88	25.06	Atkinson (1989)
3/31/82	Miramichi	22.07	24.56	Atkinson (1989)
3/31/82	Miramichi	22.07	24.73	accelerograph record
4/02/82	Miramichi	21.73	24.03	spectral ratio
4/11/82	Miramichi	21.47	23.96	spectral ratio
5/13/82	Miramichi	21.79	24.12	spectral ratio
6/16/82	Miramichi	22.44	24.43	spectral ratio
6/16/82	Miramichi	22.05	24.36	Atkinson (1989)
event 1	Nahanni	26.06	25.85	spectral ratio
event 2	Nahanni	23.32	24.60	spectral ratio
event 3	Nahanni	26.26	25.75	Choy & Boatwright (1988)
event 5	Nahanni	23.81	24.94	spectral ratio
event 6	Nahanni	23.77	24.85	spectral ratio
event 7	Nahanni	23.64	24.75	spectral ratio
event 8	Nahanni	25.49	25.55	spectral ratio
11/25/88	Saguenay	25.05	26.32	Boore & Atkinson (1989)

Units of A are dyne-cm/sec/sec.

Atkinson, 1989). To ensure that they reflect the flat portion of the acceleration spectrum (after correction for attenuation), data are included only when available for frequencies above what we take to be the corner frequency.

The data for the Miramichi aftershocks are subject to significant uncertainty because the estimates are derived from the single-station spectral ratios of Chael (1987). We only included events for which Chael also provided relative amplitudes of 8 sec surface waves. We assumed that the peak amplitude of the 8 sec waves is proportional to seismic moment, and we calculated absolute levels and seismic moments for the aftershocks, using Boore and Atkinson's (1987) compilation of moment and Boatwright and Choy's (1987; J. Boatwright, written comm., 1988) estimate of the source acceleration spectral level for the main shock. Chun et al. (1989) did not estimate the relative moments of their study events, so their results tell us nothing about absolute spectral levels. Their conclusions concerning slope, however, probably have more significance than those of Chael (1987) because of the better data quality in the Chun et al. study. We have therefore drawn the slope of the spectral level versus moment (corresponding to $\delta = 4.0$) that is implied by their analyses onto Figure 12; the level of the line is arbitrary, and was chosen to pass near the data points for the largest (i. e., best determined) Miramichi events.

A dashed line is also shown passing through the data from the Nahanni sequence. This line was determined from a regression fit to the data. The coefficients of this line give $\delta = 3.37$ and $\Delta\sigma' = 17$ bars for the scaling parameters. δ is larger than the preferred value shown in Figure 11, implying more dependence of the stress parameter on moment (log $\Delta\sigma \propto 0.16M$ versus log $\Delta\sigma \propto 0.05M$) but a stress parameter less than 35 bars for earthquakes smaller than $\mathbf{M} = 7.0$. The difference in the moment dependence of the stress is a consequence of the greater weight given the smallest events in the regression modeling as compared with the more subjective visual comparisons used in the previous derivations of the scaling parameters.

In cases where there is more than one source of spectral level or seismic moment for an event, we have plotted two connected points to show the variability of estimates. The spectral amplitudes generally appear very consistent, whether determined by analysis of regional seismographic data, teleseismic data, strong motion data, or spectral ratios (Table 3). Note, however, the significant discrepancy between the moment we estimated from Chael's (1987) data for the 6/16/82 Miramichi aftershock, and the published value from more definitive studies. This indicates that our moment estimates from Chael's data are uncertain; this is not surprising since they are estimated from a single station.

To show the implications of the data points for source scaling, we have drawn lines corresponding to stress-parameter values of 10, 50, and 100 bars in an ω-squared model. The data in Figure 12 suggest that the stress parameters for ENA main shocks scatter over the range 25 to 140 bars and have little systematic dependence on moment over a moment magnitude interval of 3.5 to 6.8. (We have ignored the Saguenay earthquake in drawing this conclusion; there is currently debate over whether this unusually deep event (30 km) should be grouped with other ENA earthquakes for evaluation of engineering design.) In contrast to the set of ENA main shocks in Figure 12, the suites of Nahanni and Miramichi earthquakes show a clear increase in stress parameter with increasing moment. There is a "shingling" of the acceleration spectral levels versus moment curves for the two sequences, the main shocks both having a stress parameter of about 30 bars, despite the difference in magnitude of the events ($\mathbf{M} = 5.5$ for Miramichi versus $\mathbf{M} = 6.8$

for Nahanni). The implication is that source scaling of aftershock sequences may not be representative of scaling for main shocks. If true, the ramifications are significant. Main shock/aftershock sequences often provide a wealth of data for a wide range of magnitudes, similar source mechanisms, and similar spatial locations. If the results cannot be generalized to a series of main shocks, they are not relevant to the prediction of ground motions in future earthquakes.

The main implication of our results for prediction of ground motion in ENA is that source spectral levels appear well represented by an ω-squared spectrum with an average stress parameter between 25 and 140 bars, for moment magnitudes of approximately 3.5 to 6.8. The ground-motion relations of Boore and Atkinson (1987), which assume a constant stress parameter of 100 bars, may be somewhat conservative, though the stress parameter for any one event might exceed 100 bars, as seems to be the case for the recent Saguenay, Quebec, earthquake.

SUMMARY

Spectral ratios for P waves have been computed from many stations for a suite of earthquakes near the Nahanni River, Northwest Territories, Canada. The earthquakes ranged from $\mathbf{M} = 4.8$ to $\mathbf{M} = 6.8$. The spectral ratios were combined with source acceleration spectra estimated by Choy and Boatwright (1988) for the largest event to obtain source acceleration spectra for all the earthquakes. Seismic moments for the smaller events were estimated from the relative amplitudes of various phases on long-period recordings at GDSN stations. The spectral ratios depend on the azimuth to the recording station, with ratios from the WCTN stations being significantly lower than those from ECTN and most GDSN stations. A likely reason for this difference is that the focal mechanisms of the earthquakes were different; rays leaving the focal sphere in the direction of the WCTN pass near a node in the P-wave radiation pattern and are thus particularly sensitive to changes in the focal mechanisms. An average of the spectral ratios obtained from the GDSN stations was taken as the best representation of the overall source radiation and was used in model fitting to obtain the source scaling for the Nahanni sequence of earthquakes.

An ω-squared source model with a constant or nearly constant stress parameter (log $\Delta\sigma \propto 0.05\mathbf{M}$) gives a reasonable simultaneous fit to the observed spectral ratios and the source acceleration spectra of the Nahanni earthquakes. The stress parameter for the preferred model is less than 25 bars for earthquakes as large as $\mathbf{M} = 7$. The ω-squared models of Nuttli (1983), Nuttli et al. (1987), and Chun et al. (1989) (for which log $\Delta\sigma \propto 0.38\mathbf{M}$) are not consistent with the data and neither are ω-cubed models (as advocated, e.g., by Evernden et al., 1986). Given the band-limited, imprecisely determined spectral ratios, nonuniqueness in the derived scaling is a serious problem if only the spectral ratios are used in the modeling or if the relative moments of the earthquakes are not available. Absolute spectral levels are important in reducing the ambiguity in conclusions concerning spectral scaling relations. For example, an ω-cubed source model gives an adequate fit to the spectral ratios if a strongly increasing stress parameter is included (log $\Delta\sigma \propto 0.56\mathbf{M}$), but the fit of the model to the acceleration spectra is atrocious. Similarly, the Nuttli (1983) and Nuttli et al. (1987) scaling predicts spectral ratios in reasonable agreement with observations, but only if the relative moments are ignored. Furthermore, as demonstrated by the comparison of the WCTN and GDSN data, spectral ratios obtained from one station (or a group of stations at similar azimuths from the

source region), even if precisely determined, can be well matched by erroneous scaling laws if there are systematic biases in the observations. The biases can be exposed by requiring a simultaneous match to both the spectral ratios and to the acceleration spectra.

Acceleration spectral levels tabulated for a number of earthquakes in ENA suggests that the average stress parameter for main shocks is independent of earthquake size, although there can be a considerable scatter in the stress parameters. In contrast, both the Miramichi, New Brunswick, and the Nahanni, Northwest Territories, main shock/aftershock sequences have a scaling such that the stress parameter increases with seismic moment. If it is generally true that the source scaling of a series of main shocks differs from that of a main shock/aftershock sequence, then spectral ratio studies, which of necessity almost always employ aftershocks, are of limited use in deriving source characteristics for the prediction of ground motions in future earthquakes.

REFERENCES

Atkinson, G. M. (1984). Attenuation of strong ground motion in Canada from a random vibrations approach, *Bull. Seism. Soc. Am.* **74**, 2629–2653.

Atkinson, G. M. (1989). Attenuation and site response for the Eastern Canada Telemetred Network, *Seism. Res. Lett.* **60**, 59–69.

Boatwright, J. and G. L. Choy (1987). Acceleration source spectra for large earthquakes in northeastern North America (abstract), *EOS* **68**, 1348.

Boore, D. M. and G. M. Atkinson (1987). Stochastic prediction of ground motion and spectral response parameters at hard-rock sites in eastern North America, *Bull. Seism. Soc. Am.* **77**, 440–467.

Boore, D. M. and G. M. Atkinson (1989). Preliminary analysis of ground motion data from the 25 November 1988 Saguenay, Quebec, earthquake (abstract), *Seism. Res. Lett.* **60**, 18.

Chael, E. P. (1987). Spectral scaling of earthquakes in the Miramichi region of New Brunswick, *Bull. Seism. Soc. Am.* **77**, 347–365.

Chael, E. P. and R. P. Kromer (1988). High-frequency spectral scaling of a main shock/aftershock sequence near the Norwegian coast, *Bull. Seism. Soc. Am.* **78**, 561–570.

Choy, G. L., J. Boatwright, J. W. Dewey, and S. A. Sipkin (1983). A teleseismic analysis of the New Brunswick earthquake of January 9, 1982, *J. Geophys. Res.* **88B**, 2199–2212.

Choy, G. L. and J. Boatwright (1988). Teleseismic and near-field analysis of the Nahanni earthquakes in the Northwest Territories, Canada, *Bull. Seism. Soc. Am.* **78**, 1627–1652.

Chun, K-Y, R. J. Kokoski, and G. F. West (1989). Source spectral characteristics of Miramichi earthquakes: results from 115 *P*-wave observations, *Bull. Seism. Soc. Am.* **79**, 15–30.

Evernden, J. F., C. B. Archambeau, and E. Cranswick (1986). An evaluation of seismic decoupling and underground nuclear test monitoring using high-frequency seismic data, *Reviews of Geophysics* **24**, 143–215.

Hanks, T. C. (1979). b values and $\omega^{-\gamma}$ seismic source models: implications for tectonic stress variations along active crustal fault zones and the estimation of high-frequency strong ground motion, *J. Geophys. Res.* **84**, 2235–2242.

Horner, R. B., R. J. Wetmiller, M. Lamontagne, and M. Plouffe (1990). A fault model for the Nahanni earthquakes from aftershock studies, *Bull. Seism. Soc. Am.* (submitted for publication).

Jenkins, G. M. and D. G. Watts (1968). *Spectral Analysis and Its Applications,* Holden-Day, San Francisco.

Nuttli, O. W. (1983). Average seismic source-parameter relations for mid-plate earthquakes, *Bull. Seism. Soc. Am.* **73**, 519–535.

Nuttli, O. W., D. S. Bowling, J. E. Lawson, Jr., and R. Wheeler (1987). Some aspects of seismic scaling and the strong ground motion of the eastern Missouri earthquake of January 12, 1984, *Seism. Res. Lett.* **58**, 53–58.

Press, W. H., B. P. Flannery, S. A. Teukolsky, and W. T. Vetterling (1986). *Numerical Recipes: The Art of Scientific Computing,* Cambridge University Press, Cambridge, England.

Street, R. L. and F. T. Turcotte (1977). A study of northeastern North American spectral moments, magnitudes, and intensities, *Bull. Seism. Soc. Am.* **67**, 599–614.

Weichert, D. H., P. W. Pomeroy, P. S. Munro, and P. N. Mork (1982). Strong motion records from Miramichi, New Brunswick, 1982 aftershocks, *Geol. Surv. Canada Earth Phys. Branch Open-File No. 82–34,* Ottawa.

Weichert, D. H., R. J. Wetmiller, and P. Munro (1986). Vertical earthquake acceleration exceeding 2 g? The case of the missing peak, *Bull. Seism. Soc. Am.* **76**, 1473–1478.

Wetmiller, R. J., R. B. Horner, H. S. Hasegawa, R. G. North, M. Lamontagne, D. H. Weichert, and S. G. Evans (1988). An analysis of the 1985 Nahanni earthquakes, *Bull. Seism. Soc. Am.* **78**, 590–616.

U. S. GEOLOGICAL SURVEY   125 DUNBAR ROAD SOUTH
MAIL STOP 977   WATERLOO, ONTARIO
345 MIDDLEFIELD ROAD   CANADA N2L 2E8
MENLO PARK, CALIFORNIA 94025   (G.M.A.)
   (D.M.B.)

APPENDIX A: SPECTRAL RATIOS AT INDIVIDUAL GDSN STATIONS

Figures A1 to A6 are plots of the spectral ratios at each GDSN station used to form the average spectra ratio. The solid line gives the ratio of the square root of the noise-corrected power spectra, with event 3 as the reference event. The ratio is plotted only when the noise-corrected power spectrum of the signal exceeds the power spectrum of the noise by a factor of 4. The dotted line is the spectral ratio averaged over the stations shown for each event. The bandwidths for the station-averaged spectral ratios were determined by the requirement that the 95 per cent confidence limits of the mean logarithm of the ratios spanned less than 0.6 log units for all frequencies within the bands. The station code, the event-to-station azimuth ("AZ," in degrees clockwise from north), and the angular distance ("D," in degrees) are given for each station. RSON and RSNY are RSTN stations. Note that for event 1 (and to a lesser extent some of the other events) the ratios are plotted up to 10 Hz, the Nyquist frequency of most of the GDSN stations, even for stations at teleseismic distances (beyond 30 degrees). This is well beyond the 2 to 3 Hz upper limit of usable *P*-wave information usually found for short-period teleseismic *P* waves (G. Choy, written comm., 1989). As explained in the text, the portions of
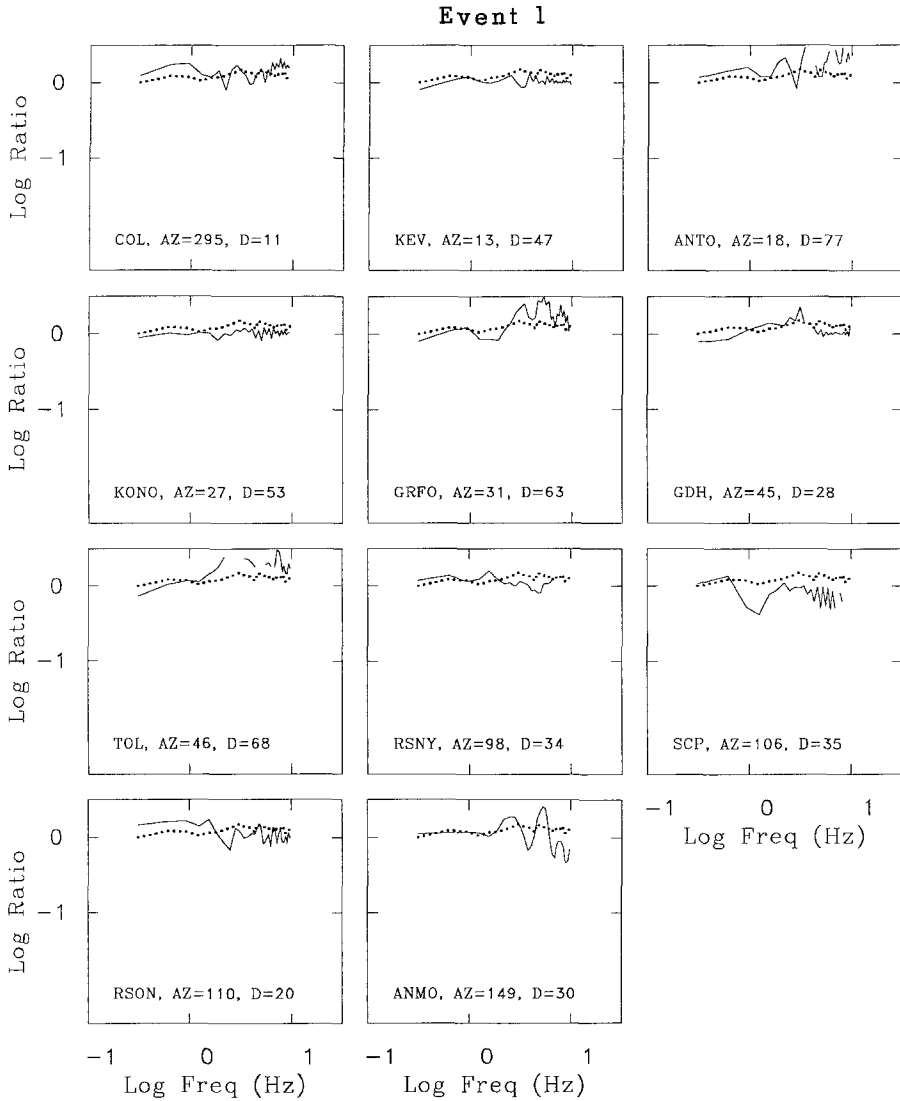
Event 1

FIG. A1. Spectral ratios for event 1.

spectra that are shown are based on a comparison of signal and noise. Furthermore, for event 1 the average spectral ratio is similar to that from WCTN and ECTN stations, and the relative excitation of low- and high-frequency motions is consistent with reported magnitudes. For all but event 1, however, the station-averaged ratios extend only up to 2 to 3 Hz, even if the ratios at a particular station may extend to higher frequencies.
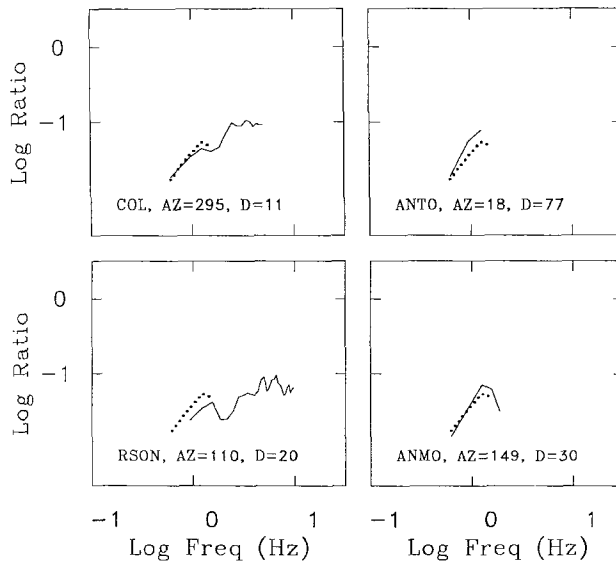
Event 2

FIG. A2. Spectral ratios for event 2.

Event 5
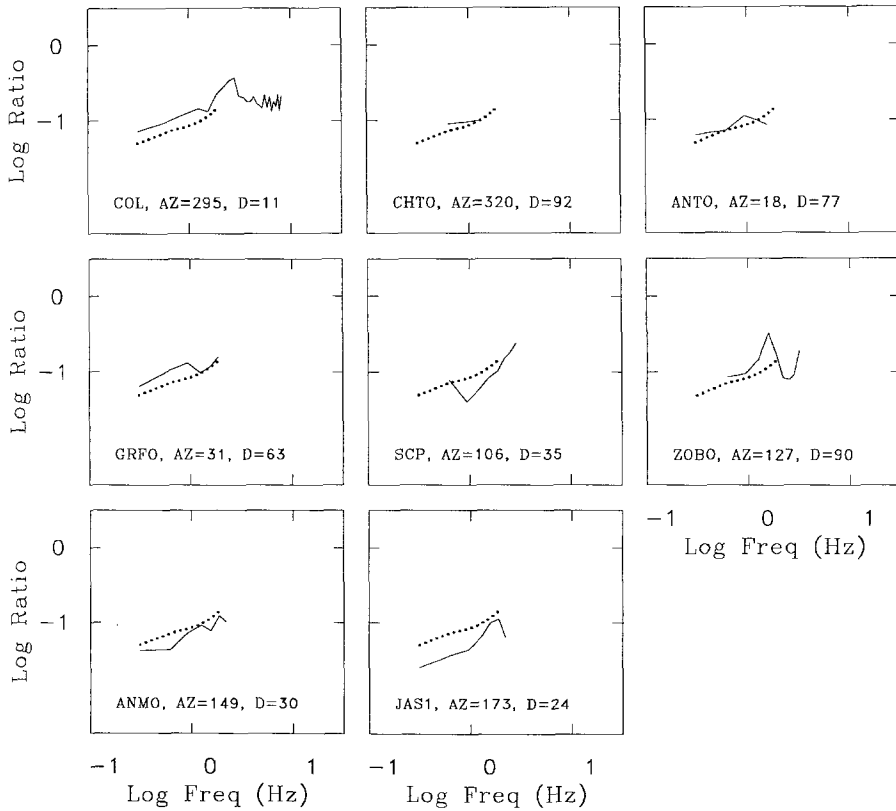
FIG. A3. Spectral ratios for event 5.
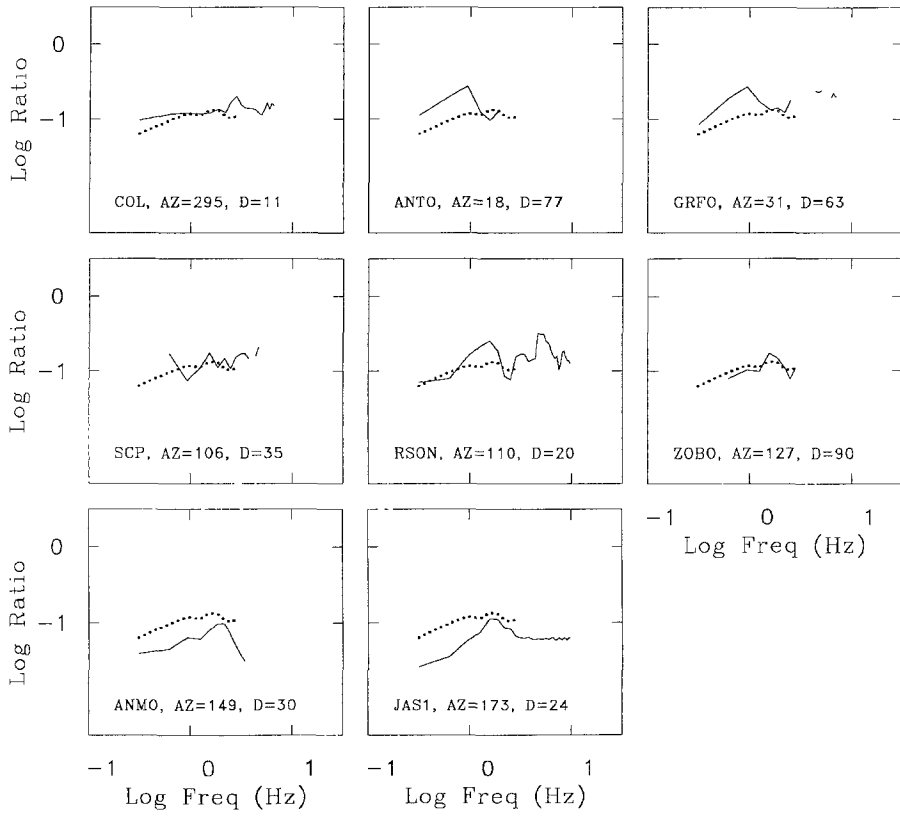
Event 6

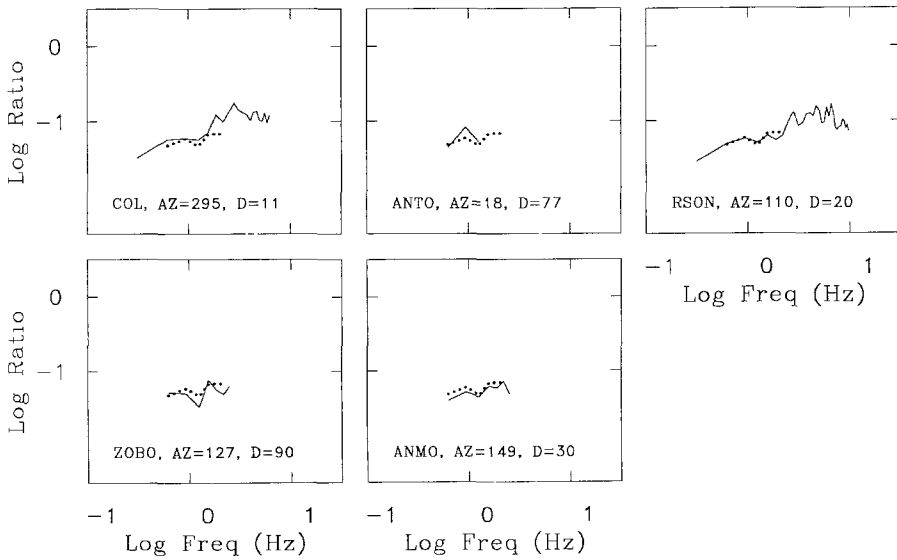FIG. A4. Spectral ratios for event 6.

Event 7

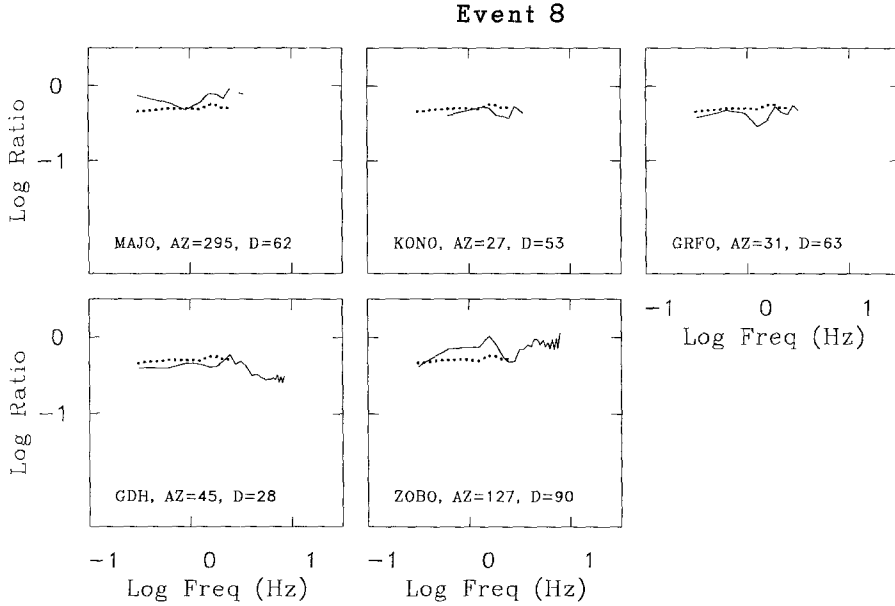

FIG. A5. Spectral ratios for event 7.

Event 8

FIG. A6. Spectral ratios for event 8.

APPENDIX B: SCALING RELATIONS

The Nuttli (1983) and Nuttli *et al.* (1987) scalings are given by the ω-squared model (equation (1)) with the corner frequency ω_0 ($2\pi f_0$) related to moment magnitude **M** according to

$$\log f_0 = -0.375\mathbf{M} + 1.538 \tag{B1}$$

for Nuttli (1983) and

$$\log f_0 = -0.375\mathbf{M} + 1.857 \tag{B2}$$

for Nuttli *et al.* (1987). The stress parameter at **M** = 5 is 6 and 60 bars for the Nuttli (1983) and Nuttli *et al.* (1987) scalings, respectively. The Boatwright and Choy scaling uses the following equations instead of equation (1) for $S(\omega)$:

$$S(\omega) = M_0/(1 + (\omega/\omega_B)^2)^{1/2} \qquad \omega \lesseqqgtr \omega_A$$

$$= M_0 \left(\frac{\omega_A}{\omega}\right) \Big/ \left(1 + \left(\frac{\omega}{\omega_B}\right)^2\right)^{1/2} \qquad \omega \gtreqqless \omega_A \tag{B3}$$

where the corner frequencies ω_A ($=2\pi f_A$) and ω_B ($=2\pi f_B$) are given by

$$\log f_A = -0.737\mathbf{M} + 3.459 \tag{B4}$$

and

$$\log f_B = -0.316\mathbf{M} + 1.694. \tag{B5}$$